Decrease in Membrane Fluidity and Traction Force Induced by Silica-Coated Magnetic Nanoparticles

Tae Hwan Shin
Ajou University School of Medicine and Graduate School of Medicine
Abdurazak Aman Ketebo
Sungkyunkwan University
Da Yeon Lee
Ajou University School of Medicine and Graduate School of Medicine
Seungah Lee
Kyung Hee University
Seong Ho Kang
Kyung Hee University
Shaherin Basith
Ajou University School of Medicine and Graduate School of Medicine
Balachandran Manavalan
Ajou University School of Medicine and Graduate School of Medicine
Sungsu Park
Sungkyunkwan University
Gwang Lee (glee@ajou.ac.kr)
Ajou University School of Medicine and Graduate School of Medicine https://orcid.org/0000-0002-1299-9478

Research

Keywords: cell movement, membrane fluidity, micropillar, silica-coated magnetic nanoparticles, traction force

Posted Date: November 12th, 2020

DOI: https://doi.org/10.21203/rs.3.rs-101142/v1

Version of Record: A version of this preprint was published on January 11th, 2021. See the published version at https://doi.org/10.1186/s12951-020-00765-5.

Abstract

Background Nanoparticles are being used increasingly due to their unique physical and chemical properties and small size. It is well-known that nanoparticles cause side effects, however their biophysical assessment remains challenging. We addressed this issue by investigating the effects of silica-coated magnetic nanoparticles containing rhodamine B isothiocyanate [MNPs@SiO_2(RITC)] on the biophysical aspects, such as membrane fluidity and traction force of human embryonic kidney 293 (HEK293) cells. We further extended our understanding on the biophysical effects of nanoparticles on cells using a combination of metabolic profiling and transcriptomic network analysis.

Results Overdose (1.0 μg/μl) treatment of MNPs@SiO_2(RITC) induced lipid peroxidation and decreased membrane fluidity in HEK293 cells. During membrane damage, HEK293 cells were morphologically shrunk and aspect ratio of the cells were significantly decreased upon MNPs@SiO_2(RITC) treatment. Each of traction force (measured in micropillar) was found to be increased, thereby increasing the total traction force in MNPs@SiO_2(RITC)-treated HEK293 cells. Due to the reduction in membrane fluidity and elevation of traction force, velocity of the cell movement was significantly decreased in MNPs@SiO_2(RITC)-treated HEK293 cells. Moreover, intracellular ATP also decreased in a dose dependent manner upon MNPs@SiO_2(RITC) treatment. To understand the biophysical changes in cells, we analysed transcriptome and metabolic profiles and generated metabotranscriptomics network. The network showed relationships among peroxidation of lipid, focal adhesion, cell movement, and related genes and metabolites. Furthermore, *in silico* prediction of the network showed increment in the peroxidation of lipid and suppression of focal adhesion and cell movement.

Conclusion Taken together, our results demonstrate that overdosage of MNPs@SiO_2(RITC) impairs cellular movement, followed by changes in the biophysical properties of cells, thus highlighting the need for biophysical assessment of nanoparticle-induced side effects.

Background

The use of nanoparticles has been rapidly increasing in medicine for diagnostic and therapeutic purposes. However, the small size of nanoparticles enables their cellular entry and accumulation, potentially causing cell dysfunction [1–4]. Moreover, compared to bulk materials, nanoparticles are more reactive and may exhibit more side effects, especially reactive oxygen species (ROS) generation, owing to their higher surface-to-volume ratio [5–7]. Nevertheless, current knowledge regarding the effects of nanoparticles on specific physical and mechanobiological aspects of a cell remains insufficient owing to the limitations of available analysis methods.

Magnetic nanoparticles (MNPs) have been commonly used as biosensors and diagnostic tools in biomedicine and biotechnology [8, 9]. MNPs are coated with biocompatible materials, such as silica and polyethyleneimine to reduce the side effects of bare MNPs [10–13]. Among the MNPs, silica-coated MNPs containing rhodamine B isothiocyanate [MNPs@SiO_2(RITC)], with layers of silica and MNP core,

are being used for separating and marking cells [12]. Based on traditional methods of toxicity evaluation, such as the chromosome aberration test, haematoxylin and eosin staining, 3-(4,5-dimethylthiazol-2-yl)-2,5-diphenyltetrazolium bromide (MTT) test, and *in vivo* tissue distribution, MNPs@SiO_2(RITC) is reportedly nontoxic [14–18]. However, MNPs@SiO_2(RITC) may exert biophysical side effects *via* ROS generation in cells [4, 17].

ROS oxidizes membranous lipids as well as cytoskeleton proteins. In particular, ROS can oxidize polyunsaturated phospholipids, glycolipids, and cholesterol in the membrane [19], thereby reducing membrane fluidity and permeability [20, 21]. In addition, internalized nanoparticles impair cytoskeleton proteins and interfere with focal adhesion kinase-mediated signaling [22]. With lamellipodia (branched actin filaments) and filopodia (extended finger-like protrusions), cell adhesions occur due to focal adhesion (FA) complexes, and cell morphology is determined through the balance between adhesion and tension [23]. The involvement of ATP in the movement of myosin over filamentous actin (F-actin) and polymerization of actin suggests that cellular mechanics can be altered by ATP depletion [24]. MNPs@SiO_2(RITC) treatment reportedly caused metabolic changes in cells, including ATP depletion [17].

Submicron elastomeric pillar array is considered an excellent tool for measuring cellular force as the nanometric level of pillar deflection can be calculated by incorporating optical microscope imaging [25, 26]. Furthermore, it can be used to analyze the initial contact of a cell with a substrate. Moreover, it reportedly mimics continuous substrates of a specific rigidity [27]. Thus, the mechanobiological effects of nanoparticles on cells could be quantitatively studied by measuring the traction force using submicron elastomeric pillars [25, 27].

The assessment of the possible side effects of nanoparticles using classical methods is limited owing to delicate changes and complexities at the nano level. Thus, instead of focusing on targeted molecules, omics approaches including genomics, transcriptomics, proteomics, and metabolomics have been used in nanotoxicity studies [18]. However, restrictions in assessing the intricate signal pathways and delicate events in cells and organisms still exist. For example, although transcriptomics can reflect enormous genotypic changes, it is insufficient for understanding the actual phenotype [28, 29]. In contrast, in the case of metabolomics, which can constitute an endpoint feature of biological phenotypes [30], no amplification methods are available for very low-abundance metabolites, and quantitative analysis of the targeted method likely provides only a partial representation of the overall metabolism [31]. Accordingly, a combination of transcriptomics and metabolomics, termed ‘metabotranscriptomics’, has been utilized to analyse nanotoxicity for a more comprehensive analysis of cells following nanoparticle treatment [4, 17, 18].

In the present study, MNPs@SiO_2(RITC)-induced effects on HEK293 cells were comprehensively evaluated *via* a biophysical assessment performed using total internal reflection fluorescence microscopy, microfabrication of pillar array, and metabotranscriptomics.

Results

MNPs@SiO_2(RITC)-induced lipid peroxidation decreases cell membrane fluidity

Here, we analyzed changes in lipid peroxidation and membrane fluidity in HEK293 cells treated with MNPs@SiO_2(RITC) at 0.1 [an adequate MNPs@SiO_2(RITC) concentration for cell labelling] and 1.0 μg/μl [a plateau concentration for the uptake of MNPs@SiO_2(RITC)] [4, 17] for 12 h, using total internal reflection fluorescence microscopy (TIRFM). Furthermore, changes in cell membrane fluidity after MNPs@SiO_2(RITC) treatment were investigated by measuring 6-dodecanoyl-2-dimethylaminonaphthalene (laurdan) generalized polarization (GP) values using TIRFM (Fig. 1a). The number of high-GP areas on the cell surface, corresponding to rigid domains, increased with MNPs@SiO_2(RITC) treatment; in particular, abundantly distributed regions of MNPs@SiO_2(RITC) primarily co-localized with high GP-distributed regions at a GP scale of -1.0 to 1.0 (Fig. 1b). GP frequency distribution values of treated cells were subtracted from the corresponding values of non-treated control cells to obtain frequency difference curves (Fig. 1c) and total mean GP values (Fig. 1d). A similar trend was observed in the relative levels of peroxidised lipid (Fig. 1e).

Moreover, a previous study revealed that MNPs@SiO_2(RITC) induced intracellular ROS generation *via* mitochondria dysfunction in HEK293 cells, with ROS generation from the shell of MNPs@SiO_2(RITC) and silica nanoparticles (silica NPs) rather than from the cobalt ferrite core when treating cells for 12 h [4, 17]. Thus, to determine intracellular ROS generation following MNPs@SiO_2(RITC) treatment, we performed 2',7'-dichlorodihydrofluorescein diacetate staining in HEK293 cells treated with 50 nm-sized silica nanoparticles, which comprise the same material and size of the shell of MNPs@SiO_2(RITC). The intracellular ROS level was increased by over 50% upon 1.0 μg/μl silica-NP treatment compared to that in non-treated control and 0.1 μg/μl silica-NP-treated cells (See Supplementary Figure 1, Additional File 1), a finding consistent with that of previous reports [4, 17]. These results indicated that the rigid regions in the plasma membrane increased through lipid peroxidation induced by ROS generated from the shell of MNPs@SiO_2(RITC).

MNPs@SiO_2(RITC)-treatment decreases cell polarity and spread area but increases traction force

As membrane fluidity is closely related to cell morphology as well as focal adhesion [32, 33], we investigated whether a decrease in membrane fluidity mediated by MNPs@SiO_2(RITC) also affects cell morphology and focal adhesion. We then evaluated the effects of MNPs@SiO_2(RITC) on cell polarity as local cell contraction is tightly associated with these activities along with changes in focal adhesion [34]. Moreover, the cell aspect ratio was measured. Images of cells and submicron pillars at 12 h were analysed after cell seeding (Fig. 2a, b). The aspect ratio of the cells at 0.1 μg/μl MNPs@SiO_2(RITC) did not significantly differ from that of the non-treated control cells, although the ratio of the cells treated with 1.0 μg/μl MNPs@SiO_2(RITC) was significantly smaller than that of the non-treated control cells (Fig. 2c).

Pillar deflection in the magnified images was used to measure pillar displacement (Fig. 2d) and calculate traction force (Fig. 2e, f). To calculate pillar traction force, the displacement of each pillar was multiplied with the pillar bending stiffness [27]. In particular, 1.0 μg/μl MNPs@SiO_2(RITC)-treated cells showed a significant increase in pillar displacement (351 ± 65 nm; mean ± SD), which was significantly higher than that of the non-treated control cells (216 ± 46 nm). Average (8.5 ± 2 nN) and total (1112 ± 197 nN) traction forces of 1.0 μg/μl MNPs@SiO_2(RITC) cells were significantly higher than those (5.2 ± 1 and 855 ± 172 nN) of the non-treated control cells, indicating that cell traction force was affected by 1.0 μg/μl MNPs@SiO_2(RITC). Taken together, the increase in cell traction force results from MNPs@SiO_2(RITC) treatment-induced reduction in cell polarity and spread area.

MNPs@SiO_2(RITC)-treatment impairs cell movement

We previously analysed the effect of MNPs@SiO_2(RITC) treatment on the migratory activity of human bone marrow-derived mesenchymal stem cells (hBM-MSCs). The impairment of migratory activity was observed in hBM-MSCs using conventional assays, such as wound healing and invasion assays [35]. To evaluate the biophysical changes related to the biological functions of HEK293, we analysed the effect of 0.1 or 1.0 μg/μl MNPs@SiO_2(RITC) on HEK293 cell movement using conventional assays. In the wound healing assay, no difference was observed in terms of the migratory activity between MNPs@SiO_2(RITC)-treated HEK293 cells and non-treated control cells (Fig. 3a). Similarly, no difference was observed in invasion ability, analysed using transwell invasion assay, between MNPs@SiO_2(RITC)-treated HEK293 cells and non-treated control cells (Fig. 3b).

The aforementioned results of the wound healing and invasion assays do not exclude the cell growth effect and treatment of growth-arrest agents such as mitomycin C, as the assays are highly toxic to HEK293 cells [36]. Thus, we analysed individual cells' movement by tracking cells on pillars for 24 h after treating them with MNPs@SiO_2(RITC) for 12 h on a dish (Additional File 2: Movie S1, Movie S2, and Movie S3). The distances traveled by the cells were significantly decreased to a greater extent for MNPs@SiO_2(RITC)-treated HEK293 cells than for non-treated control at 6 and 24 h (Fig. 3c). Similar result was observed for movement speeds at 6 h and 24 h (Fig. 3d).

MNPs@SiO_2(RITC)-treatment decreases intracellular ATP level

To evaluate the changes in intracellular ATP level of MNPs@SiO_2(RITC)-treated cells, HEK293 cells were treated with MNPs@SiO_2(RITC) at 0 to 2.0 μg/μl for 6, 12, and 24 h (Fig. 4). Intracellular ATP levels were decreased in a dose-dependent manner in MNPs@SiO_2(RITC)-treated cells starting from 0.13 μg/μl dose. Moreover, the decrement pattern was similar at 6, 12, and 24 h treatment.

Metabotranscriptomic network of MNPs@SiO_2(RITC)-treated HEK293 cells

To analyse the dispersed phenomena of MNPs@SiO_2(RITC)-treated cells, a co-expression network of gene and metabolites was constructed using a transcriptome generated from microarray analysis and the

metabolome derived from amino acid and organic acid profiling using Ingenuity Pathway Analysis (IPA, http://www.ingenuity.com) [17]. Microarray expression analysis showed that the levels of 21 genes associated with lipid peroxidation and those of 31 genes related to focal adhesion formation were altered in MNPs@SiO_2(RITC)-treated cells (Fig. 5a, b). In the transcriptomic network with changes determined using a 3-fold cut-off only, more pronounced changes were detected in 1.0 μg/μl MNPs@SiO_2(RITC)-treated cells than in 0.1 μg/μl MNPs@SiO_2(RITC)-treated cells and control cells; these changes were related to cell movement (Fig. 5c, See Supplementary Figures 2, Additional File 1). The *in-silico* prediction of the network revealed activation of lipid peroxidation as well as suppression of focal adhesion and cell movement in 1.0 μg/μl MNPs@SiO_2(RITC)-treated HEK293 cells (Fig. 5d).

Although transcriptomics provided comprehensive information regarding MNPs@SiO_2(RITC)-treated cells, the data were qualitative. Thus, for evaluating network-based analysis, we used a combination of transcriptome and metabolome networks, termed the metabotranscriptomic network, through the substitution of amino acid and organic acid profiles (cut-off ± 20% change), as described in our previous report [17]. In the group treated with 1.0 μg/μl MNPs@SiO_2(RITC), amino acid, organic acid, and free fatty acid profiles showed increased levels of tyrosine, pyruvic acid, glutamic acid, lysine and lignoceric acid; in contrast, decreased levels of cysteine, asparagine, 3-hydroxybutyric acid, glutamine, serine, aspartic acid, oxaloacetic acid, glycine, and acetoacetic acid were observed [37]. The combined network provided more reliable information than the transcriptomic network alone, with more pronounced changes also being detected in 1.0 μg/μl than in 0.1 μg/μl MNPs@SiO_2(RITC)-treated cells and control cells (Fig. 6a; Supplementary Figures 3, Supplementary Table 1, Additional File 1).μl The *in-silico* prediction of the integrated network also showed similar trend of transcriptome network (See Supplementary Figure 4, Additional File 1).

The expression levels of genes associated with the network were subsequently quantified using semiquantitative reverse transcription PCR (Fig. 6b) and quantitative (q) PCR (Fig. 6c). In particular, the expression levels of superoxide dismutase 2 (*SOD2*) and LIM zinc finger domain-containing 1 (*LIMS1*) were increased, whereas those of NCK adaptor protein 1 (*NCK1*) and complement C3a receptor 1 (*C3AR1*) were decreased in the 1.0 μg/μl MNPs@SiO_2(RITC)-treated cells relative to those in the non-treated control cells.

Discussion

The present study demonstrates the effects of nanoparticles on the biophysical properties of cells. In addition, functional analysis with the metabotranscriptomics approach helped us deduce interconnective relationships between genes and metabolites associated with lipid peroxidation, focal adhesion, and cell movement in MNPs@SiO_2(RITC)-treated cells.

We observed that the 1.0 μg/μl MNPs@SiO_2(RITC)-treated cells exhibited markedly increased lipid peroxidation levels than the non-treated control and 0.1 μg/μl MNPs@SiO_2(RITC)-treated cells. These

results indicated that exposure of cells to 1.0 μg/μl of MNPs@SiO_2(RITC) may impair certain biological functions due to ROS production and lipid peroxidation. This is consistent with the findings that oxidative stress induces lipid peroxidation, which is often observed in disease states, such as aging, sickle-cell disease, malaria, and diabetes [38–40]. It also conforms to the decrease in hBM-MSC deformability over time owing to intracellular ROS generation and lipid peroxidation, which leads to decreased membrane fluidity and deteriorated cell quality [41]. Moreover, we previously showed that ROS-distributed regions distinctly co-localized with the MNPs@SiO_2(RITC)-distributed regions in cells [17]; hence, abundantly distributed regions of MNPs@SiO_2(RITC) might be primarily co-localized with high GP-distributed regions along with lipid peroxidation, indicating damaged membrane regions. Thus, our results suggest that exposure of cells to 1.0 μg/μl MNPs@SiO_2(RITC) potentially impairs the biological functions of exposed cells *via* increased membrane rigidity.

Cell membrane damage induced by nanoparticles is reportedly caused *via* direct interactions between membrane lipids and nanoparticles [42]. Silica and gold nanoparticles are known to penetrate cell membranes [43, 44]. In particular, 50 nm MNPs@SiO_2(RITC)s were likely internalized through endocytic pathways because nanoparticles > 10 nm are coated directly with the plasma membrane and are internalized *via* the clathrin- and caveolae-mediated endocytic pathways [45, 46]; altered gene expression of the clathrin-mediated endocytic pathway significantly altered the internalization of MNPs@SiO_2(RITC)s in HEK293 cells and SH-SY5Y neuroblastoma cells [4]. Thus, we propose that MNPs@SiO_2(RITC) enters the cells by endocytosis; this constitutes one reason for decreased membrane fluidity, because membrane tension regulates membrane deformation or a change in cell shape (e.g. endocytosis, exocytosis, cytokinesis, and cell motility) [47].

Besides the membrane damage caused by nanoparticles, the status of cell membranes is highly linked to cytoskeleton regulation, because the membrane and cytoskeleton are tightly associated with phosphoinositides [48, 49]. Nanoparticle-induced lipid peroxidation reportedly alters cell morphology and membrane roughness in human lymphocytes [50]. Cell aspect ratio and cell spread area were decreased in MNPs@SiO_2(RITC)-treated cells with round morphology, suggesting that focal adhesion was impaired owing to the imbalance between adhesion and tension caused by MNPs@SiO_2(RITC) treatment.

Nanoparticles reportedly increase traction force but inhibit cellular migration [51]. Traction force is primarily regulated by the phosphorylation of myosin II through the assembly (dephosphorylated myosin) and disassembly (phosphorylated myosin) of myosin light chain (also termed the myosin head) and actin filaments, with these processes obtaining energy from ATP hydrolysis [52, 53]. Our previous study showed that the intracellular level of ATP in 1.0 μg/μl MNPs@SiO_2(RITC)-treated cells was decreased to approximately 50% *via* mitochondrial damage [17]. In the present study, MNPs@SiO_2(RITC) treatment decreased intracellular ATP levels in dose- and time-dependent manners, and this may be the one of the factors responsible for the increment of the total traction force and reduction in cell movement activity.

In the transcriptome network associated with lipid peroxidation, focal adhesion, and cell movement, there were limitations in terms of interpreting the actual phenotype. Thus, datasets of differentially expressed genes and metabolites were combined, providing information to clarify the interactions between differentially expressed genes and altered metabolites, thereby generating a metabotranscriptomic network. In particular, the network showed that the expression levels of *SOD2*, which is tightly associated with oxidative stress [54], and *LIMS1*, which is an important molecule in the linkage between actin and integrin for the formation of focal adhesions [55], were increased, whereas the levels of *NCK1*, an upstream regulator in the formation of actin-rich protrusions in the plasma membrane [56], and *C3AR1*, known to be reduced in oxidative conditions [57, 58], were decreased in the 1.0 μg/μl MNPs@SiO_2(RITC)-treated cells relative to those in the non-treated controls. Thus, the convergence of the metabolic profiles and transcriptome disturbances allows an interpretation of the changes in the movement of MNPs@SiO_2(RITC)-treated cells.

Conclusions

In conclusion, our results demonstrated reduction in membrane fluidity, abnormal focal adhesion, and decrement in cell movement upon treatment with a high (1.0 μg/μl) concentration of MNPs@SiO_2(RITC). Our findings indicate that nanoparticles should be used at a dosage as low as possible in therapeutic or diagnostic applications for preventing potential nanotoxicity. Our comprehensive approach for toxicological evaluation will aid the future assessment of nanoparticle sensitivity and the associated potential toxicity. Moreover, our findings of nanotoxicity will be beneficial in terms of the development of safe nanoparticles for biomedical applications.

Materials And Methods

MNPs@SiO_2(RITC) and silica NPs

The MNPs@SiO_2(RITC) consisted of an approximately 9-nm cobalt ferrite core ($CoFe_2O_3$) chemically bonded to rhodamine isothiocyanate dye (RITC) and coated with a silica shell [12]. Silica nanoparticles are identical to the silica shell of MNPs@SiO_2(RITC), and the biological effects show a similar trend as that exhibited by MNPs@SiO_2(RITC) [4, 16, 17]. The diameter of MNPs@SiO_2(RITC) and silica nanoparticles is 50 nm (See Supplementary Figure 5, Additional File 1), with MNPs@SiO_2(RITC)s reported to have a *zeta* potential of −40 to −30 mV [12, 16]. A previous study showed that approximately 10^5 particles of MNPs@SiO_2(RITC) per cell were internalized in MCF-7 breast cancer cells, as determined using inductively coupled plasma atomic emission spectrometry [12]. The dosage used in the present study was determined by treating HEK293 cells with MNPs@SiO_2(RITC) at concentrations ranging from 0.01 to 2.0 μg/μl for 12 h and calculating their uptake efficiencies [17]. The optimal concentration of MNPs@SiO_2(RITC) for *in vitro* use was determined as 0.1 μg/μl; this concentration had been used for MRI contrast without any reported toxicological effects in human cord blood-derived mesenchymal stem cells [59]. Disturbances in gene expression and metabolic profiles of the treated cells at this concentration

were similar to those of the control cells [17]. The uptake efficiency of MNPs@SiO_2(RITC) plateaued at 1.0 μg/μl. Therefore, a low dose of 0.1 μg/μl and high dose of 1.0 μg/μl were used in the present study.

Measurement of membrane fluidity

Changes in membrane fluidity were measured using laurdan, a fluorescence dye that exhibits a 60-nm spectral shift from disordered to ordered bilayer phases, and an in-house combined differential interference contrast-total internal reflection fluorescence microscopy experimental system (DIC-TIRFM) [41, 60]. The procedure was based on a well-described protocol [41, 61, 62]. Briefly, cells were seeded on cover slips (no. 1 thickness, 0.13–0.16 mm) and treated with 0.1 and 1.0 μg/μl MNPs@SiO_2(RITC) for 12 h. For staining with laurdan, cells were incubated with medium containing 10 μM laurdan in a 37°C incubator at 5% CO_2 for 2 h. The cells were washed twice with phosphate buffered saline (PBS) and fixed with fixation buffer (Cytofix; BD, San Jose, CA, USA). Cover slips containing cells were mounted onto other cover slips (no. 1 thickness, 0.13–0.16 mm) with mounting medium (Prolong gold antifade; Molecular Probes, Eugene, OR, USA). Cell morphological changes, laurdan fluorescence, and MNPs@SiO_2(RITC) distribution were observed using an oil-type 100× objective lens (Olympus UPLFL 100×/1.3 N.A., W.D. 0.1 mm, Tokyo, Japan) and a CCD camera (QuantEM 512SC, Photometrics, Tucson, AZ, USA). Laurdan was excited at 405 nm, and emission fluorescence was detected with 420 nm and 473 nm bandpass filters (resolution: ± 5 nm). As a parameter of membrane fluidity, GP [($Intensity_{420\ nm}$ − $Intensity_{473\ nm}$) / ($Intensity_{420\ nm}$ + $Intensity_{473\ nm}$)] was calculated and pseudo-coloured; GP images merged with DIC images were generated using Image J software (NIH, Bethesda, MD, USA) [63]. Gaussian distributions were generated using the nonlinear fitting algorithm in Sigma plot 10.0 (Systat Software Inc., San Jose, CA, USA).

Microfabrication of submicron elastomeric pillar array

Photolithography was used to fabricate a silicon wafer mould with a series of holes [64]. To make the pillars, PDMS was mixed in a 10:1 ratio with its curing agent (Sylgard 184; Dow Corning, Midland, MI, USA) and vacuumed for 15 min; the mould was then spin-coated with PDMS at 1,000 RPM for 1 min and again vacuumed to remove bubbles for 30 min. The mould with PDMS was cured at 80°C for 3 h. Using this method, the pillar array was manufactured. Each pillar was 900 nm in diameter (*D*), 1 μm in height (*L*), and 1.8 μm in centre-to-centre distance. To calculate the bending stiffness (*k*) of the pillar, the Euler–Bernoulli beam theory was applied [27]:

$$k = \frac{3}{64}\pi E \frac{D^4}{L^3}$$

where *E* is the Young's modulus (2 MPa) of the cured PDMS. With this equation, *k* of the pillar was calculated to be 24.2 nN/μm.

Measurement of cell aspect ratio

The cell aspect ratio was measured by representing the area of the entire cell with a comparable elliptical shape using ImageJ (NIH); the division from the major axis of the ellipse to the minor axis was then taken as the cell aspect ratio.

Measurement of traction force

Pillar images were acquired using a fluorescence microscope (Deltavision, GE Healthcare, Chicago, IL, USA) and a camera (CoolSNAP HQ^2, Photometrics) at 37°C and 5% humidity with a live cell chamber at 1 Hz. The location of each pillar in each frame was determined using the pillar tracking plugin (PillarTracker 1.1.3 version) for ImageJ. In the pillar reconstruction algorithm, the PillarTracker works to establish the exact grid of the pillar array, thereby allowing users to automatically detect and track the locations of pillars. Throughout this study, the pillars that had no contact with cells were used as reference pillars. To account for stage drift, the average displacement of the reference pillars was deducted from the displacement data of the pillars deflected by cells. To avoid the unwanted displacement of pillars by MNPs@SiO_2(RITC), MNPs@SiO_2(RITC)-treated cells were washed five times using PBS (Sigma-Aldrich, St. Louis, MO, USA) before seeding onto the pillar array. The displacement of each pillar was multiplied with its bending stiffness to calculate the traction force (F).

Metabotranscriptomic data analysis

Differences in the gene expression of cells were examined using the Affymetrix system (ISTECH, South Korea) in conjunction with the Human U133 Plus 2.0 50K microarray, which contains 54,675 probes. Differences in the data distribution were analysed using GenPlex 3.0 software [17], and the probe signals were quantile normalized. Amino acid and organic acid profiles were imported from previously reported data [17]. Biological pathways and functions were identified using the web-based bioinformatics software Ingenuity pathway analysis (IPA; Ingenuity Systems, Redwood City, CA, USA). A 3-fold change in gene expression and 20% change in metabolites were used as cut-offs to generate datasets of significantly altered genes and metabolites.

Cell tracking

The PDMS pillars were coated with fibronectin for 1 h before seeding the cells. The cells were then seeded at a density of 3000 cells per sample and tracked every 5 min for 6 h on a JuLi™ Br live cell movie analyser (NanoEntek, Inc., Seoul, Korea). Finally, the cell movement speed was calculated by tracking cells using ImageJ software.

Statistical analysis and error correction

The results were analysed by one-way analysis of variance (ANOVA) with Bonferroni's multiple-comparison test using IBM-SPSS software (IBM Corp., Armonk, NY, USA). $p < 0.05$ was considered statistically significant. In the experiments using micropillars, errors in the pillar deflections were corrected by reducing the average pillar deflection of pillars outside the cell.

Declarations

Funding

This work was supported by the research (2018R1D1A1B07049494), (2018R1A2B2002066), BioNano Health-Guard Research Center Grant (H-GUARD_2018M3A6B2057299), (2020R1C1C1008366), (2020R1A4A4079722), (2020M3E5D9080661), (2016M3C7A1904392) through the National Research Foundation funded by the Ministry of Science and ICT (MSIP) of Korea.

Authors' Contributions

THS, AAK, SP, and GL conceived and designed the experiments. THS and AAK performed the experiments and analysed the data. SL and SHK performed the lab-built microscopy system. DYL performed the cell experiments of NPs in cells. BM and SB helped with experimental design, and data analysis. THS, AAK, SP, and GL drafted the paper. All of the authors read and approved the final manuscript.

Corresponding authors

Correspondence to Sungsu Park or Gwang Lee.

Ethics declarations

Ethics approval and consent to participate

Not applicable.

Consent for publication

Not applicable.

Competing interests

The authors declare that they have no competing interests.

Acknowledgments

The authors would like to thank the Ajou Core-Facility Center and Sun Young Che for technical assistance and cell image analysis.

Author information

Tae Hwan Shin and Abdurazak Aman Ketebo contributed equally to this work.

Affiliations

Department of Physiology and Department of Biomedical Sciences, Ajou University School of Medicine, Suwon, 16499, Republic of Korea

Tae Hwan Shin, Da Yeon Lee, Shaherin Basith, Balachandran Manavalan & Gwang Lee

School of Mechanical Engineering, Sungkyunkwan University, Suwon, 16419, Republic of Korea

Abdurazak Aman Ketebo & Sungsu Park

Department of Chemistry, Graduate School, Kyung Hee University, Yongin-si, 17104, Republic of Korea

Seungah Lee & Seung Ho Kang

Department of Molecular Science and Technology, Ajou University, Suwon, 16499, Republic of Korea

Gwang Lee

References

1. Xia T, Kovochich M, Liong M, Madler L, Gilbert B, Shi H, Yeh JI, Zink JI, Nel AE: **Comparison of the mechanism of toxicity of zinc oxide and cerium oxide nanoparticles based on dissolution and oxidative stress properties.***ACS Nano* 2008, **2:**2121-2134.
2. Nel AE, Madler L, Velegol D, Xia T, Hoek EM, Somasundaran P, Klaessig F, Castranova V, Thompson M: **Understanding biophysicochemical interactions at the nano-bio interface.***Nat Mater* 2009, **8:**543-557.
3. Krug HF, Wick P: **Nanotoxicology: an interdisciplinary challenge.***Angew Chem Int Ed Engl* 2011, **50:**1260-1278.
4. Phukan G, Shin TH, Shim JS, Paik MJ, Lee JK, Choi S, Kim YM, Kang SH, Kim HS, Kang Y, et al: **Silica-coated magnetic nanoparticles impair proteasome activity and increase the formation of cytoplasmic inclusion bodies in vitro.***Sci Rep* 2016, **6:**29095.
5. Nel A, Xia T, Madler L, Li N: **Toxic potential of materials at the nanolevel.***Science* 2006, **311:**622-627.
6. Auffan M, Rose J, Bottero JY, Lowry GV, Jolivet JP, Wiesner MR: **Towards a definition of inorganic nanoparticles from an environmental, health and safety perspective.***Nat Nanotechnol* 2009, **4:**634-641.
7. Liu R, Liu HH, Ji Z, Chang CH, Xia T, Nel AE, Cohen Y: **Evaluation of Toxicity Ranking for Metal Oxide Nanoparticles via an in Vitro Dosimetry Model.***ACS Nano* 2015, **9:**9303-9313.
8. Akbarzadeh A, Samiei M, Davaran S: **Magnetic nanoparticles: preparation, physical properties, and applications in biomedicine.***Nanoscale Res Lett* 2012, **7:**144.
9. Belanova AA, Gavalas N, Makarenko YM, Belousova MM, Soldatov AV, Zolotukhin PV: **Physicochemical Properties of Magnetic Nanoparticles: Implications for Biomedical Applications In Vitro and In Vivo.***Oncol Res Treat* 2018, **41:**139-143.

10. Zhou Y, Tang Z, Shi C, Shi S, Qian Z, Zhou S: **Polyethylenimine functionalized magnetic nanoparticles as a potential non-viral vector for gene delivery.***J Mater Sci Mater Med* 2012, **23:**2697-2708.
11. Uthaman S, Lee SJ, Cherukula K, Cho CS, Park IK: **Polysaccharide-Coated Magnetic Nanoparticles for Imaging and Gene Therapy.***Biomed Res Int* 2015, **2015:**959175.
12. Yoon TJ, Kim JS, Kim BG, Yu KN, Cho MH, Lee JK: **Multifunctional nanoparticles possessing a "magnetic motor effect" for drug or gene delivery.***Angew Chem Int Ed Engl* 2005, **44:**1068-1071.
13. Ding YF, Li S, Liang L, Huang Q, Yuwen L, Yang W, Wang R, Wang LH: **Highly Biocompatible Chlorin e6-Loaded Chitosan Nanoparticles for Improved Photodynamic Cancer Therapy.***ACS Appl Mater Interfaces* 2018, **10:**9980-9987.
14. Kim JS, Yoon TJ, Yu KN, Kim BG, Park SJ, Kim HW, Lee KH, Park SB, Lee JK, Cho MH: **Toxicity and tissue distribution of magnetic nanoparticles in mice.***Toxicol Sci* 2006, **89:**338-347.
15. Park KS, Tae J, Choi B, Kim YS, Moon C, Kim SH, Lee HS, Kim J, Kim J, Park J, et al: **Characterization, in vitro cytotoxicity assessment, and in vivo visualization of multimodal, RITC-labeled, silica-coated magnetic nanoparticles for labeling human cord blood-derived mesenchymal stem cells.***Nanomedicine* 2010, **6:**263-276.
16. Beck GR, Jr., Ha SW, Camalier CE, Yamaguchi M, Li Y, Lee JK, Weitzmann MN: **Bioactive silica-based nanoparticles stimulate bone-forming osteoblasts, suppress bone-resorbing osteoclasts, and enhance bone mineral density in vivo.***Nanomedicine* 2012, **8:**793-803.
17. Shim W, Paik MJ, Nguyen DT, Lee JK, Lee Y, Kim JH, Shin EH, Kang JS, Jung HS, Choi S, et al: **Analysis of changes in gene expression and metabolic profiles induced by silica-coated magnetic nanoparticles.***ACS Nano* 2012, **6:**7665-7680.
18. Shin TH, Lee DY, Lee HS, Park HJ, Jin MS, Paik MJ, Manavalan B, Mo JS, Lee G: **Integration of metabolomics and transcriptomics in nanotoxicity studies.***BMB Rep* 2018, **51:**14-20.
19. Girotti AW: **Lipid hydroperoxide generation, turnover, and effector action in biological systems.***J Lipid Res* 1998, **39:**1529-1542.
20. Cazzola R, Rondanelli M, Russo-Volpe S, Ferrari E, Cestaro B: **Decreased membrane fluidity and altered susceptibility to peroxidation and lipid composition in overweight and obese female erythrocytes.***J Lipid Res* 2004, **45:**1846-1851.
21. de la Haba C, Palacio JR, Martinez P, Morros A: **Effect of oxidative stress on plasma membrane fluidity of THP-1 induced macrophages.***Biochim Biophys Acta* 2013, **1828:**357-364.
22. Soenen SJ, Nuytten N, De Meyer SF, De Smedt SC, De Cuyper M: **High intracellular iron oxide nanoparticle concentrations affect cellular cytoskeleton and focal adhesion kinase-mediated signaling.***Small* 2010, **6:**832-842.
23. Hall A: **Rho GTPases and the actin cytoskeleton.***Science* 1998, **279:**509-514.
24. Kuhner S, Fischer S: **Structural mechanism of the ATP-induced dissociation of rigor myosin from actin.***Proc Natl Acad Sci U S A* 2011, **108:**7793-7798.

25. Tan JL, Tien J, Pirone DM, Gray DS, Bhadriraju K, Chen CS: **Cells lying on a bed of microneedles: an approach to isolate mechanical force.***Proc Natl Acad Sci U S A* 2003, **100:**1484-1489.
26. du Roure O, Saez A, Buguin A, Austin RH, Chavrier P, Silberzan P, Ladoux B: **Force mapping in epithelial cell migration.***Proc Natl Acad Sci U S A* 2005, **102:**2390-2395.
27. Ghassemi S, Meacci G, Liu S, Gondarenko AA, Mathur A, Roca-Cusachs P, Sheetz MP, Hone J: **Cells test substrate rigidity by local contractions on submicrometer pillars.***Proc Natl Acad Sci U S A* 2012, **109:**5328-5333.
28. Evans TG: **Considerations for the use of transcriptomics in identifying the 'genes that matter' for environmental adaptation.***J Exp Biol* 2015, **218:**1925-1935.
29. Rehrauer H, Opitz L, Tan G, Sieverling L, Schlapbach R: **Blind spots of quantitative RNA-seq: the limits for assessing abundance, differential expression, and isoform switching.***BMC Bioinformatics* 2013, **14:**370.
30. Gibney MJ, Walsh M, Brennan L, Roche HM, German B, van Ommen B: **Metabolomics in human nutrition: opportunities and challenges.***Am J Clin Nutr* 2005, **82:**497-503.
31. Van Assche R, Broeckx V, Boonen K, Maes E, De Haes W, Schoofs L, Temmerman L: **Integrating -Omics: Systems Biology as Explored Through C. elegans Research.***J Mol Biol* 2015, **427:**3441-3451.
32. Gaus K, Le Lay S, Balasubramanian N, Schwartz MA: **Integrin-mediated adhesion regulates membrane order.***J Cell Biol* 2006, **174:**725-734.
33. Sun M, Northup N, Marga F, Huber T, Byfield FJ, Levitan I, Forgacs G: **The effect of cellular cholesterol on membrane-cytoskeleton adhesion.***J Cell Sci* 2007, **120:**2223-2231.
34. Notbohm J, Banerjee S, Utuje KJC, Gweon B, Jang H, Park Y, Shin J, Butler JP, Fredberg JJ, Marchetti MC: **Cellular Contraction and Polarization Drive Collective Cellular Motion.***Biophys J* 2016, **110:**2729-2738.
35. Shin TH, Lee DY, Ketebo AA, Lee S, Manavalan B, Basith S, Ahn C, Kang SH, Park S, Lee G: **Silica-Coated Magnetic Nanoparticles Decrease Human Bone Marrow-Derived Mesenchymal Stem Cell Migratory Activity by Reducing Membrane Fluidity and Impairing Focal Adhesion.***Nanomaterials (Basel)* 2019, **9:**1475.
36. Hsieh JH, Huang R, Lin JA, Sedykh A, Zhao J, Tice RR, Paules RS, Xia M, Auerbach SS: **Real-time cell toxicity profiling of Tox21 10K compounds reveals cytotoxicity dependent toxicity pathway linkage.***PLoS One* 2017, **12:**e0177902.
37. Shin TH, Seo C, Lee DY, Ji M, Manavalan B, Basith S, Chakkarapani SK, Kang SH, Lee G, Paik MJ, Park CB: **Silica-coated magnetic nanoparticles induce glucose metabolic dysfunction in vitro via the generation of reactive oxygen species.***Archives of Toxicology* 2019, **93:**1201-1212.
38. Chien S: **Red cell deformability and its relevance to blood flow.***Annu Rev Physiol* 1987, **49:**177-192.
39. Mohanty JG, Nagababu E, Rifkind JM: **Red blood cell oxidative stress impairs oxygen delivery and induces red blood cell aging.***Front Physiol* 2014, **5:**84.

40. Hierso R, Waltz X, Mora P, Romana M, Lemonne N, Connes P, Hardy-Dessources MD: **Effects of oxidative stress on red blood cell rheology in sickle cell patients.***Br J Haematol* 2014, **166:**601-606.
41. Shin TH, Lee S, Choi KR, Lee DY, Kim Y, Paik MJ, Seo C, Kang S, Jin MS, Yoo TH, et al: **Quality and freshness of human bone marrow-derived mesenchymal stem cells decrease over time after trypsinization and storage in phosphate-buffered saline.***Sci Rep* 2017, **7:**1106.
42. Van Lehn RC, Ricci M, Silva PH, Andreozzi P, Reguera J, Voitchovsky K, Stellacci F, Alexander-Katz A: **Lipid tail protrusions mediate the insertion of nanoparticles into model cell membranes.***Nat Commun* 2014, **5:**4482.
43. Lin J, Zhang H, Chen Z, Zheng Y: **Penetration of lipid membranes by gold nanoparticles: insights into cellular uptake, cytotoxicity, and their relationship.***ACS Nano* 2010, **4:**5421-5429.
44. Mu Q, Hondow NS, Krzeminski L, Brown AP, Jeuken LJ, Routledge MN: **Mechanism of cellular uptake of genotoxic silica nanoparticles.***Part Fibre Toxicol* 2012, **9:**29.
45. Oh N, Park JH: **Endocytosis and exocytosis of nanoparticles in mammalian cells.***Int J Nanomedicine* 2014, **9 Suppl 1:**51-63.
46. Wang Z, Tiruppathi C, Minshall RD, Malik AB: **Size and dynamics of caveolae studied using nanoparticles in living endothelial cells.***ACS Nano* 2009, **3:**4110-4116.
47. Nambiar R, McConnell RE, Tyska MJ: **Control of cell membrane tension by myosin-I.***Proc Natl Acad Sci U S A* 2009, **106:**11972-11977.
48. Saarikangas J, Zhao H, Lappalainen P: **Regulation of the actin cytoskeleton-plasma membrane interplay by phosphoinositides.***Physiol Rev* 2010, **90:**259-289.
49. Geissler KJ, Jung MJ, Riecken LB, Sperka T, Cui Y, Schacke S, Merkel U, Markwart R, Rubio I, Than ME, et al: **Regulation of Son of sevenless by the membrane-actin linker protein ezrin.***Proc Natl Acad Sci U S A* 2013, **110:**20587-20592.
50. Zhornik EV, Baranova LA, Drozd ES, Sudas MS, Chau NH, Buu NQ, Dung TT, Chizhik SA, Volotovskii ID: **[Silver nanoparticles induce lipid peroxidation and morphological changes in human lymphocytes surface].***Biofizika* 2014, **59:**466-473.
51. Tay CY, Cai P, Setyawati MI, Fang W, Tan LP, Hong CH, Chen X, Leong DT: **Nanoparticles strengthen intracellular tension and retard cellular migration.***Nano Lett* 2014, **14:**83-88.
52. Kasza KE, Farrell DL, Zallen JA: **Spatiotemporal control of epithelial remodeling by regulated myosin phosphorylation.***Proc Natl Acad Sci U S A* 2014, **111:**11732-11737.
53. Gerthoffer WT, Schaafsma D, Sharma P, Ghavami S, Halayko AJ: **Motility, survival, and proliferation.***Compr Physiol* 2012, **2:**255-281.
54. Mohanty JG, Nagababu E, Friedman JS, Rifkind JM: **SOD2 deficiency in hematopoietic cells in mice results in reduced red blood cell deformability and increased heme degradation.***Exp Hematol* 2013, **41:**316-321.
55. Humphrey JD, Dufresne ER, Schwartz MA: **Mechanotransduction and extracellular matrix homeostasis.***Nat Rev Mol Cell Biol* 2014, **15:**802-812.

56. Yamaguchi H, Lorenz M, Kempiak S, Sarmiento C, Coniglio S, Symons M, Segall J, Eddy R, Miki H, Takenawa T, Condeelis J: **Molecular mechanisms of invadopodium formation: the role of the N-WASP-Arp2/3 complex pathway and cofilin.***J Cell Biol* 2005, **168:**441-452.
57. Zhao W, Zhao T, Chen Y, Qu Y, Gerling IC, Sun Y: **Modification of oxidative stress on gene expression profiling in the rat infarcted heart.***Mol Cell Biochem* 2013, **379:**243-253.
58. Rutar M, Natoli R, Albarracin R, Valter K, Provis J: **670-nm light treatment reduces complement propagation following retinal degeneration.***J Neuroinflammation* 2012, **9:**257.
59. Park KS, Tae J, Choi B, Kim YS, Moon C, Kim SH, Lee HS, Kim J, Park J, Lee JH, et al: **Characterization, in vitro cytotoxicity assessment, and in vivo visualization of multimodal, RITC-labeled, silica-coated magnetic nanoparticles for labeling human cord blood-derived mesenchymal stem cells.***Nanomedicine : nanotechnology, biology, and medicine* 2010, **6:**263-276.
60. Lee S, Cho NP, Kim JD, Jung H, Kang SH: **An ultra-sensitive nanoarray chip based on single-molecule sandwich immunoassay and TIRFM for protein detection in biologic fluids.***Analyst* 2009, **134:**933-938.
61. Owen DM, Rentero C, Magenau A, Abu-Siniyeh A, Gaus K: **Quantitative imaging of membrane lipid order in cells and organisms.***Nat Protoc* 2012, **7:**24-35.
62. Schneckenburger H, Stock K, Strauss WS, Eickholz J, Sailer R: **Time-gated total internal reflection fluorescence spectroscopy (TG-TIRFS): application to the membrane marker laurdan.***J Microsc* 2003, **211:**30-36.
63. Hansen JS, Helix-Nielsen C: **An epifluorescence microscopy method for generalized polarization imaging.***Biochem Biophys Res Commun* 2011, **415:**686-690.
64. Tan JL, Liu W, Nelson CM, Raghavan S, Chen CS: **Simple approach to micropattern cells on common culture substrates by tuning substrate wettability.***Tissue Eng* 2004, **10:**865-872.

Figures

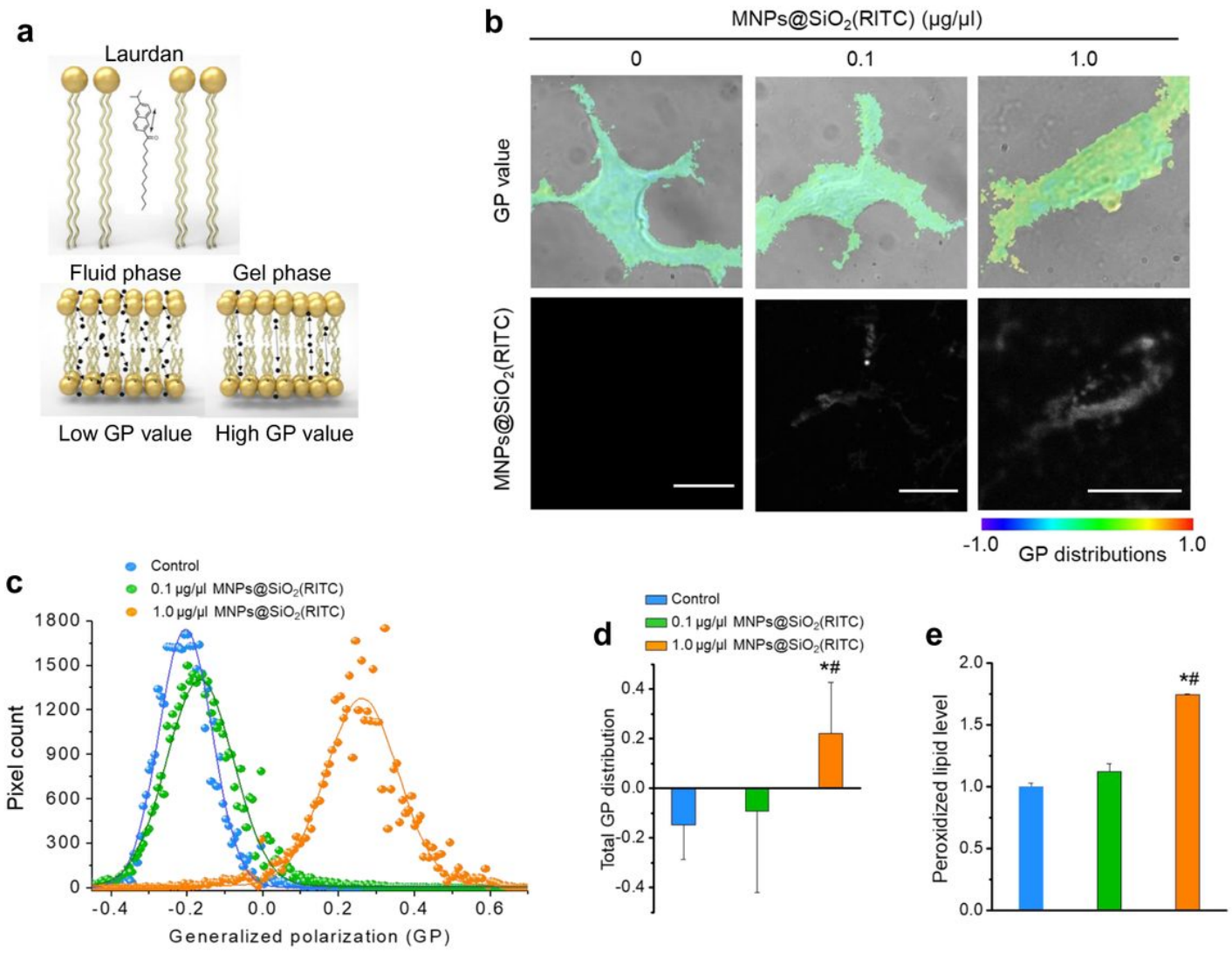

Figure 1

Laurdan GP images and GP frequency distributions of MNPs@SiO2(RITC)-treated HEK293 cells. (a) Schematic representation of laurdan usage for measuring the GP value of membrane. (b) Merged DIC and TIRFM images (left panel) of HEK293 cells. Distributions of MNPs@SiO2(RITC) are shown in each right panel. GP distributions ranged from −1.0 to 1.0. Scale bar = 2.5 μm. (c) GP frequency distributions of cells. GP values of each pixel are represented as dots and were fitted to Gaussian distributions. (d) Total GP values. Data represent the means ± SD of three independent experiments (N = 10). (e) Evaluation of peroxidised lipids using ferrous thiocyanate. The intensity of ferrous thiocyanate only was used as the blank. Data represent the means ± SD of three independent experiments. *p < 0.05 vs non-treated control, #p < 0.05 compared between 0.1 and 1.0 μg/μl MNPs@SiO2(RITC)-treated cells.

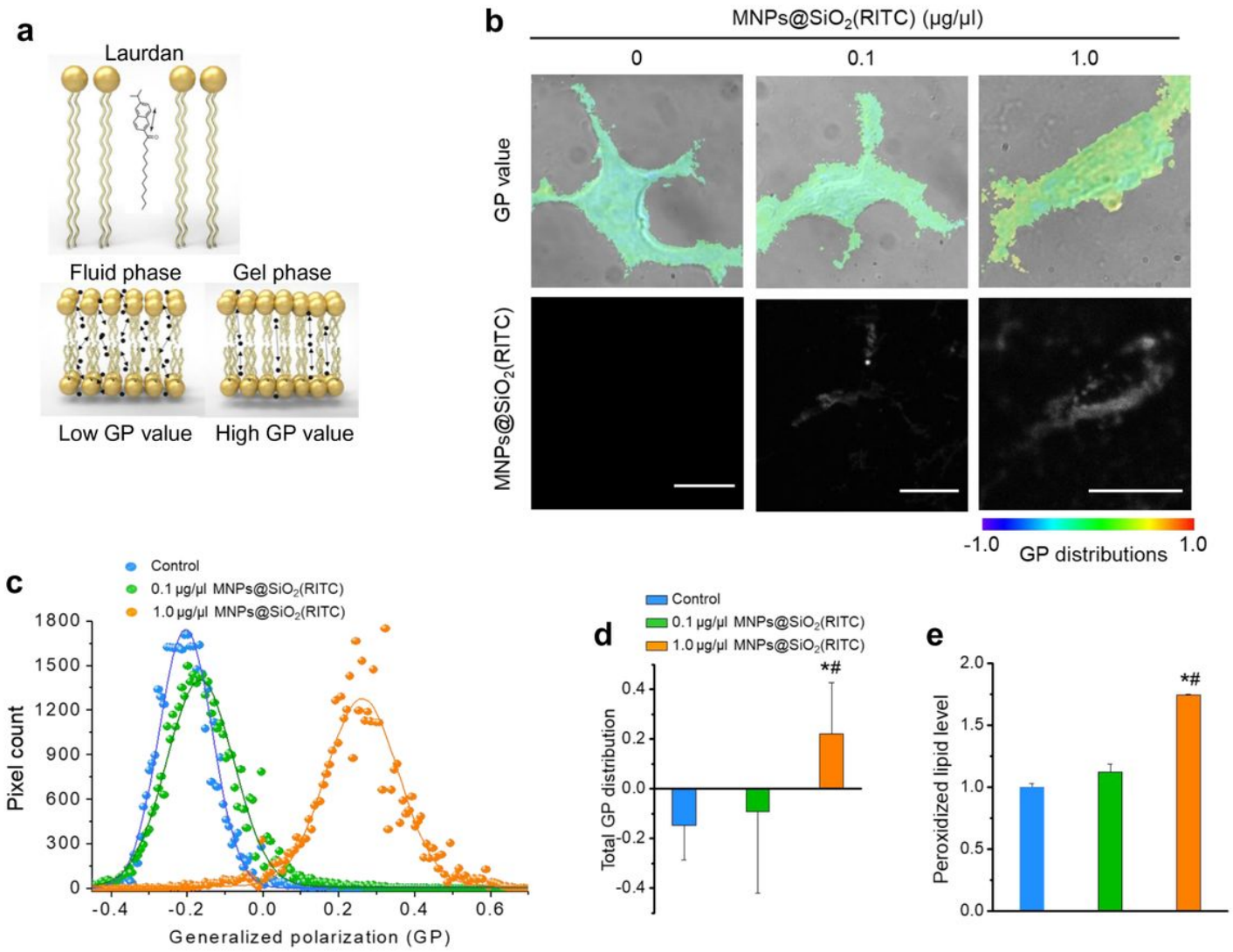

Figure 1

Laurdan GP images and GP frequency distributions of MNPs@SiO2(RITC)-treated HEK293 cells. (a) Schematic representation of laurdan usage for measuring the GP value of membrane. (b) Merged DIC and TIRFM images (left panel) of HEK293 cells. Distributions of MNPs@SiO2(RITC) are shown in each right panel. GP distributions ranged from −1.0 to 1.0. Scale bar = 2.5 μm. (c) GP frequency distributions of cells. GP values of each pixel are represented as dots and were fitted to Gaussian distributions. (d) Total GP values. Data represent the means ± SD of three independent experiments (N = 10). (e) Evaluation of peroxidised lipids using ferrous thiocyanate. The intensity of ferrous thiocyanate only was used as the blank. Data represent the means ± SD of three independent experiments. *p < 0.05 vs non-treated control, #p < 0.05 compared between 0.1 and 1.0 μg/μl MNPs@SiO2(RITC)-treated cells.

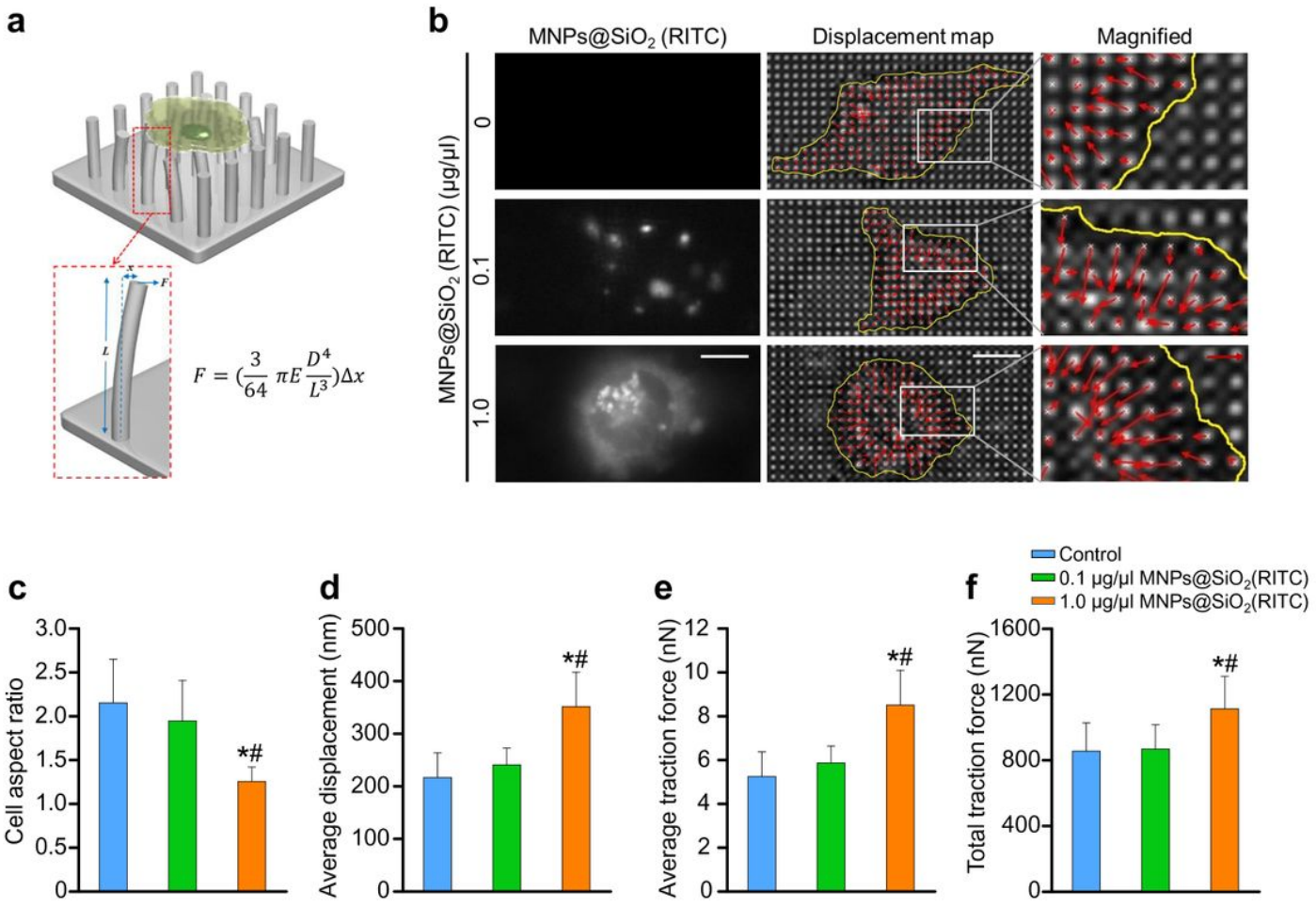

Figure 2

Change in pillar deflection, traction force, aspect ratio, and surface area of MNPs@SiO2(RITC)-treated HEK293 cells. (a) Schematic drawing of the measurement traction force (F) of cells treated with MNPs@SiO2(RITC) using submicron elastomeric micropillars. (b) Representative images presenting the concentration of MNPs@SiO2(RITC) inside the cell, pillar deflections, and magnified pillar deflections at the edge of the cell (left to right). Red arrows represent pillar deflection, and the white bar represents 8 μm. Yellow lines indicate the approximate cell boundary. Direction and length of the red arrow indicate the magnitude and direction of pillar deflection, respectively. (c) Aspect ratio of cells spread over the pillar array. (d) Spreading area of cells over the pillar array. (e) Average displacement of each pillar under the cell. (f) Average traction force of each pillar under the cell and (g) total traction force of pillars beneath the cell. Data represent the means ± SD. *p < 0.05 vs non-treated control. #p < 0.05 compared between 0.1 and 1.0 μg/μl MNPs@SiO2(RITC)-treated cells.

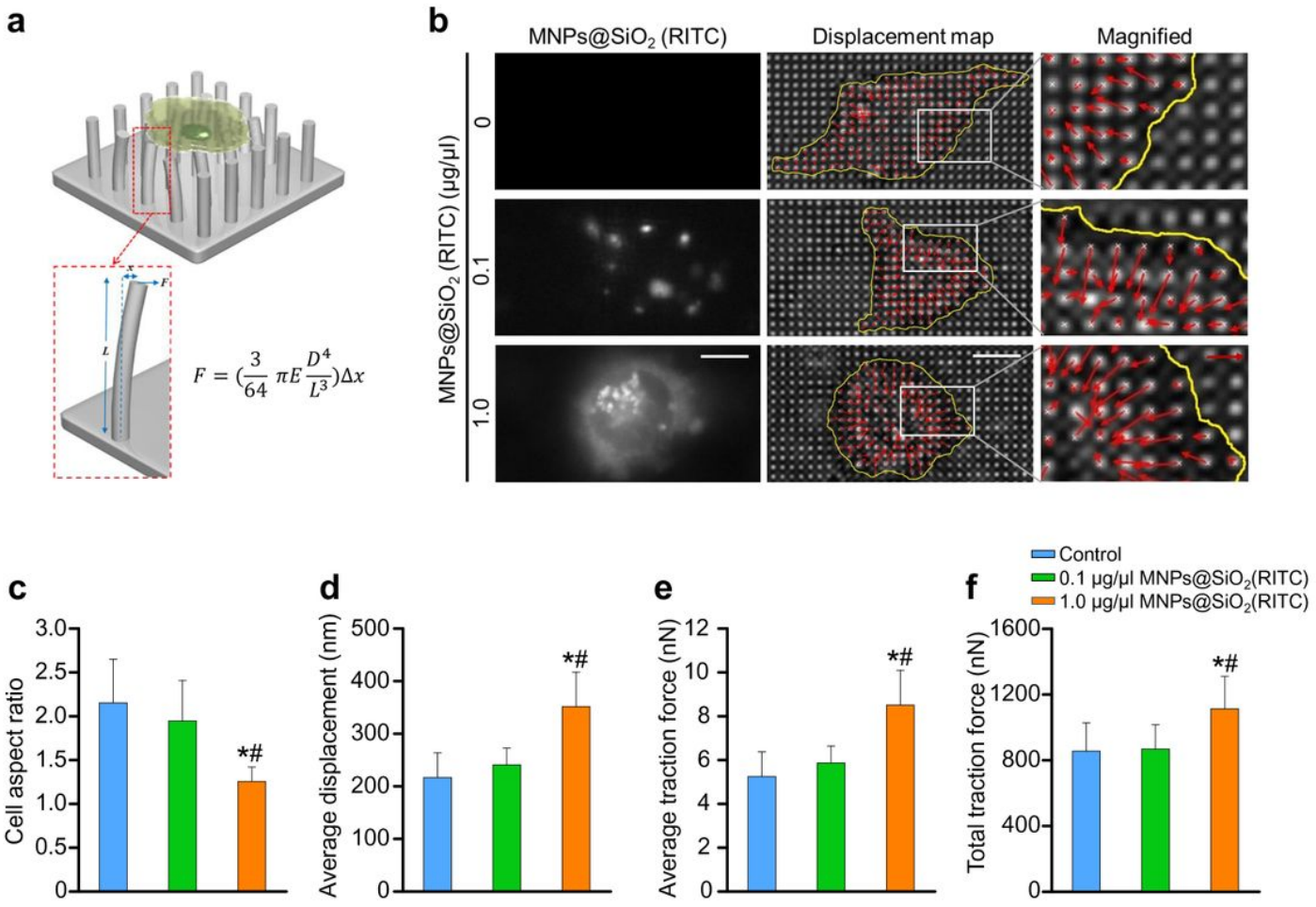

Figure 2

Change in pillar deflection, traction force, aspect ratio, and surface area of MNPs@SiO2(RITC)-treated HEK293 cells. (a) Schematic drawing of the measurement traction force (F) of cells treated with MNPs@SiO2(RITC) using submicron elastomeric micropillars. (b) Representative images presenting the concentration of MNPs@SiO2(RITC) inside the cell, pillar deflections, and magnified pillar deflections at the edge of the cell (left to right). Red arrows represent pillar deflection, and the white bar represents 8 μm. Yellow lines indicate the approximate cell boundary. Direction and length of the red arrow indicate the magnitude and direction of pillar deflection, respectively. (c) Aspect ratio of cells spread over the pillar array. (d) Spreading area of cells over the pillar array. (e) Average displacement of each pillar under the cell. (f) Average traction force of each pillar under the cell and (g) total traction force of pillars beneath the cell. Data represent the means ± SD. *p < 0.05 vs non-treated control. #p < 0.05 compared between 0.1 and 1.0 μg/μl MNPs@SiO2(RITC)-treated cells.

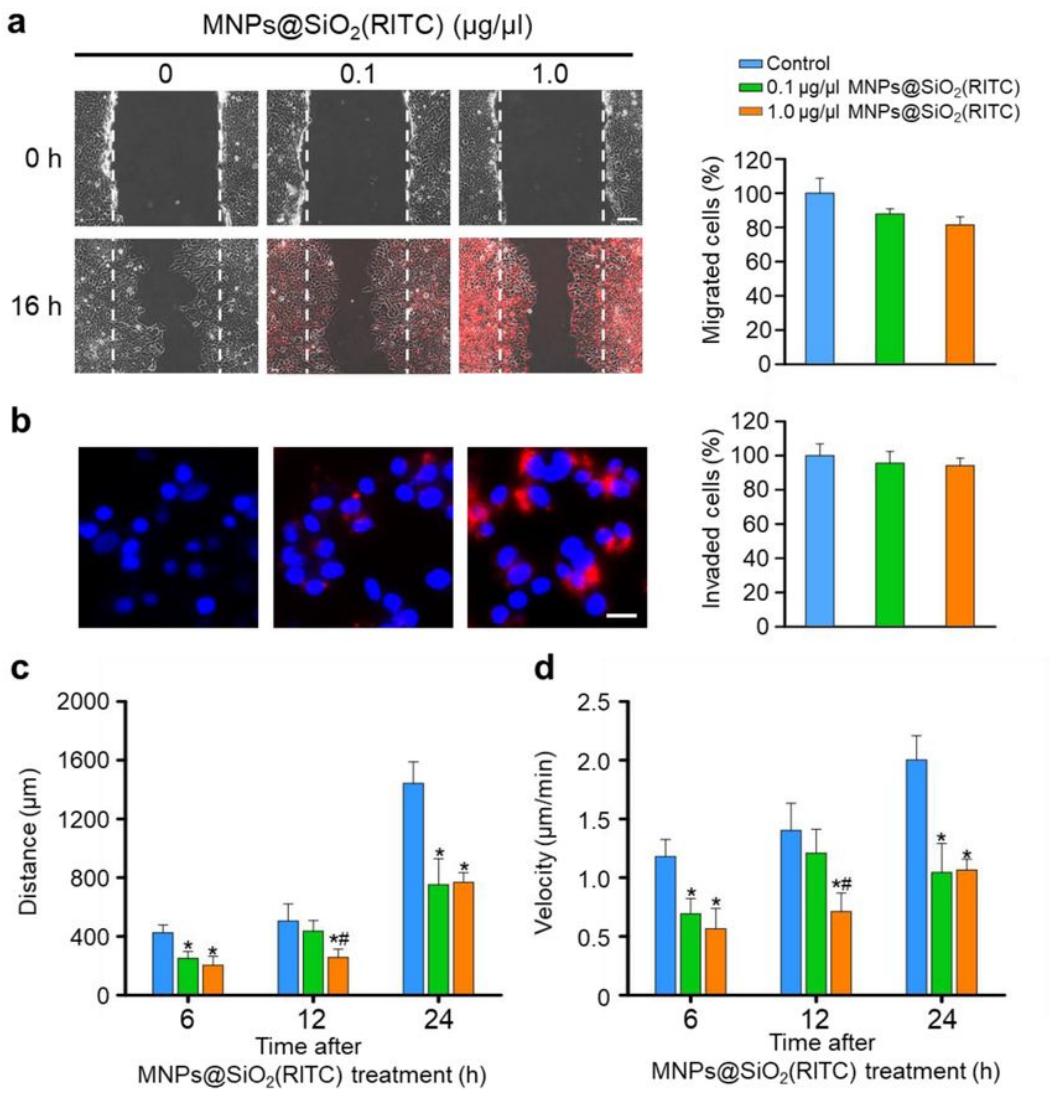

Figure 3

Evaluation of the movement of MNPs@SiO2(RITC)-treated HEK293 cells. (a) Representative images of the wound healing assay and quantitative image analysis. Images of the initial wounded (0 h) layer are shown in the upper panels. Images of HEK293 cells after MNPs@SiO2(RITC) treatment for 16 h are shown in the lower panels. Scale bar = 100 μm. Quantitative image analysis of migrated cells in MNPs@SiO2(RITC)-treated HEK293 cells are shown in the bar graph. (b) Representative images of the HEK293 cells and quantitative image analysis of the invasion assay results after MNPs@SiO2(RITC) treatment for 12 h. Red, MNPs@SiO2(RITC); blue, Hoechst 33342. Scale bar = 20 μm. Quantitative image analysis of invaded MNPs@SiO2(RITC)-treated HEK293 cells are shown in the bar graph. Individual cell tracking analysis for travel distance (c) and velocity (d) of MNPs@SiO2(RITC)-treated HEK293 cells at 6, 12, and 24 h. Data represent mean ± SD of three independent experiments. *p < 0.05 vs. non-treated control, #p < 0.05 for the comparison between cells treated with 0.1 and 1.0 μg/μl of MNPs@SiO2(RITC).

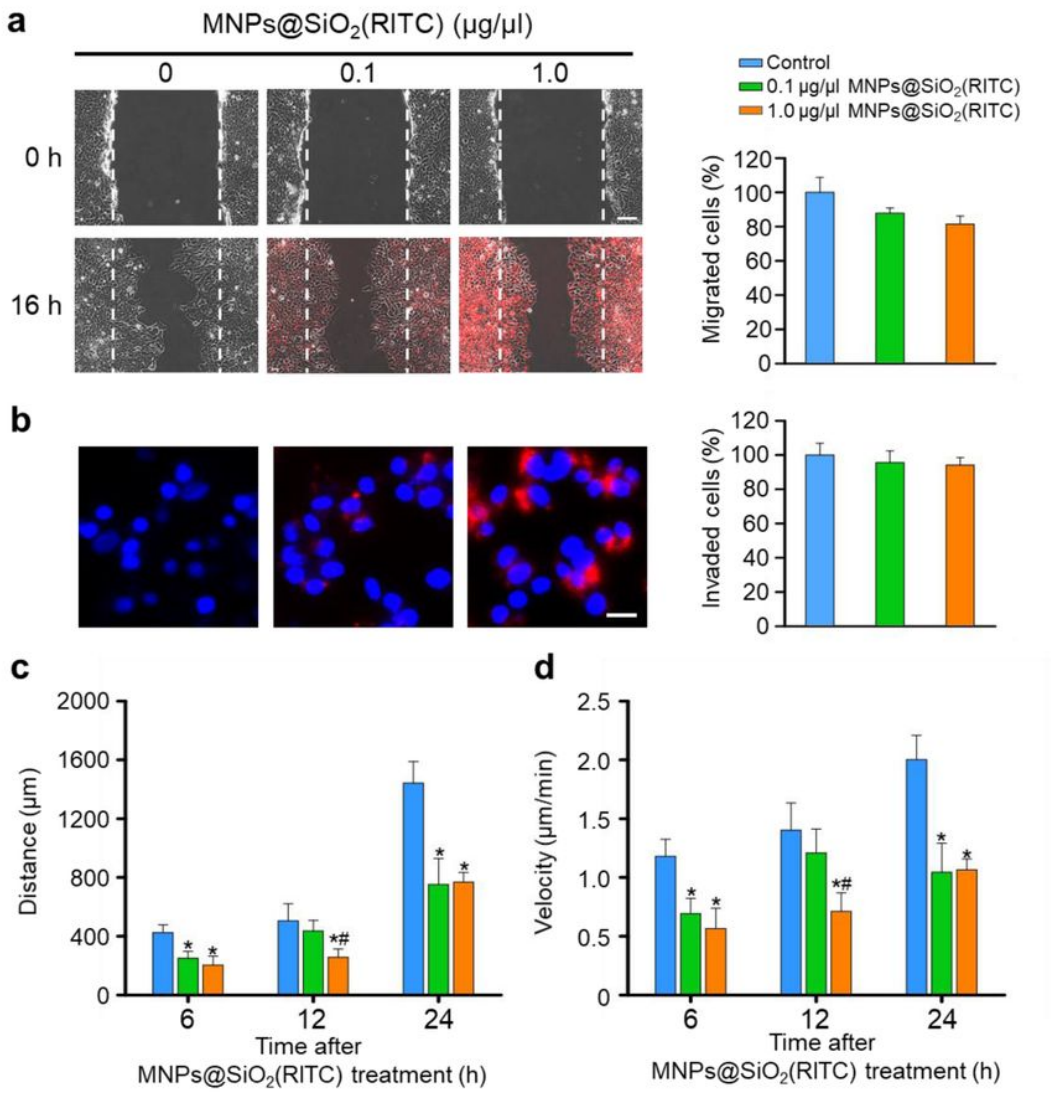

Figure 3

Evaluation of the movement of MNPs@SiO2(RITC)-treated HEK293 cells. (a) Representative images of the wound healing assay and quantitative image analysis. Images of the initial wounded (0 h) layer are shown in the upper panels. Images of HEK293 cells after MNPs@SiO2(RITC) treatment for 16 h are shown in the lower panels. Scale bar = 100 μm. Quantitative image analysis of migrated cells in MNPs@SiO2(RITC)-treated HEK293 cells are shown in the bar graph. (b) Representative images of the HEK293 cells and quantitative image analysis of the invasion assay results after MNPs@SiO2(RITC) treatment for 12 h. Red, MNPs@SiO2(RITC); blue, Hoechst 33342. Scale bar = 20 μm. Quantitative image analysis of invaded MNPs@SiO2(RITC)-treated HEK293 cells are shown in the bar graph. Individual cell tracking analysis for travel distance (c) and velocity (d) of MNPs@SiO2(RITC)-treated HEK293 cells at 6, 12, and 24 h. Data represent mean ± SD of three independent experiments. *p < 0.05 vs. non-treated control, #p < 0.05 for the comparison between cells treated with 0.1 and 1.0 μg/μl of MNPs@SiO2(RITC).

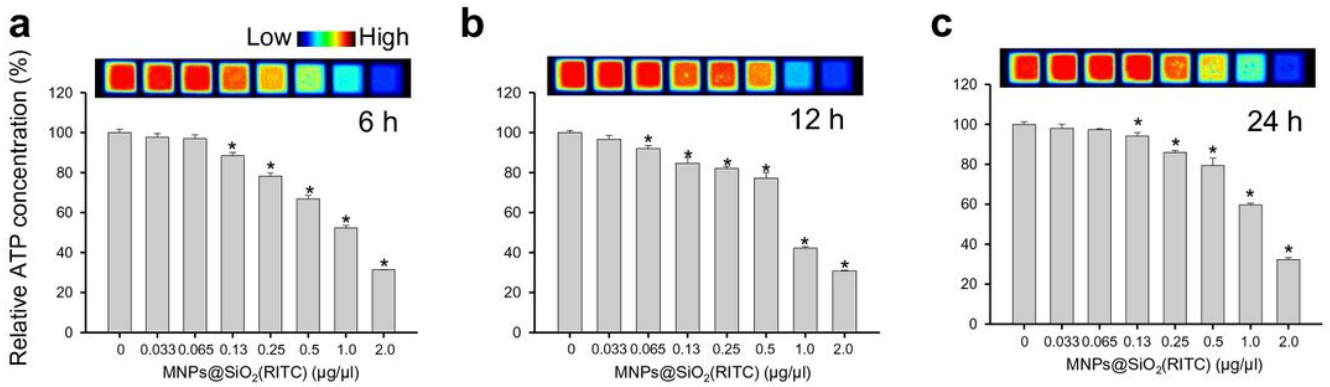

Figure 4

Evaluation of intracellular ATP level in MNPs@SiO2(RITC)-treated HEK293 cells. HEK293 cells were treated with 0 to 2.0 μg/μl MNPs@SiO2(RITC) for (a) 6, (b) 12, and (c) 24 h and intracellular ATP level were analysed. The luminance was captured and expressed as pseudocolor scale image. Data represent mean ± SD of three independent experiments. *p < 0.05 vs. non-treated control, #p < 0.05 for the comparison between cells treated with 0.1 and 1.0 μg/μl of MNPs@SiO2(RITC).

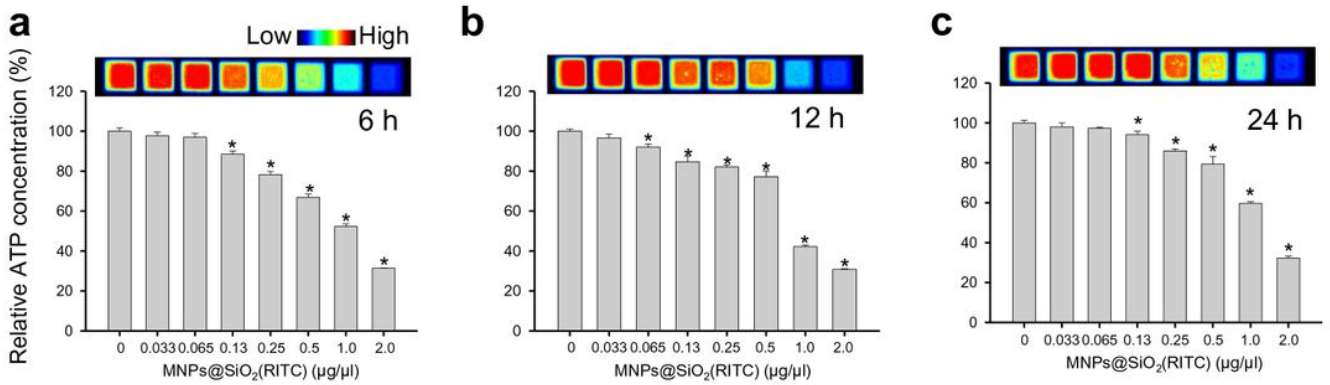

Figure 4

Evaluation of intracellular ATP level in MNPs@SiO2(RITC)-treated HEK293 cells. HEK293 cells were treated with 0 to 2.0 μg/μl MNPs@SiO2(RITC) for (a) 6, (b) 12, and (c) 24 h and intracellular ATP level were analysed. The luminance was captured and expressed as pseudocolor scale image. Data represent mean ± SD of three independent experiments. *p < 0.05 vs. non-treated control, #p < 0.05 for the comparison between cells treated with 0.1 and 1.0 μg/μl of MNPs@SiO2(RITC).

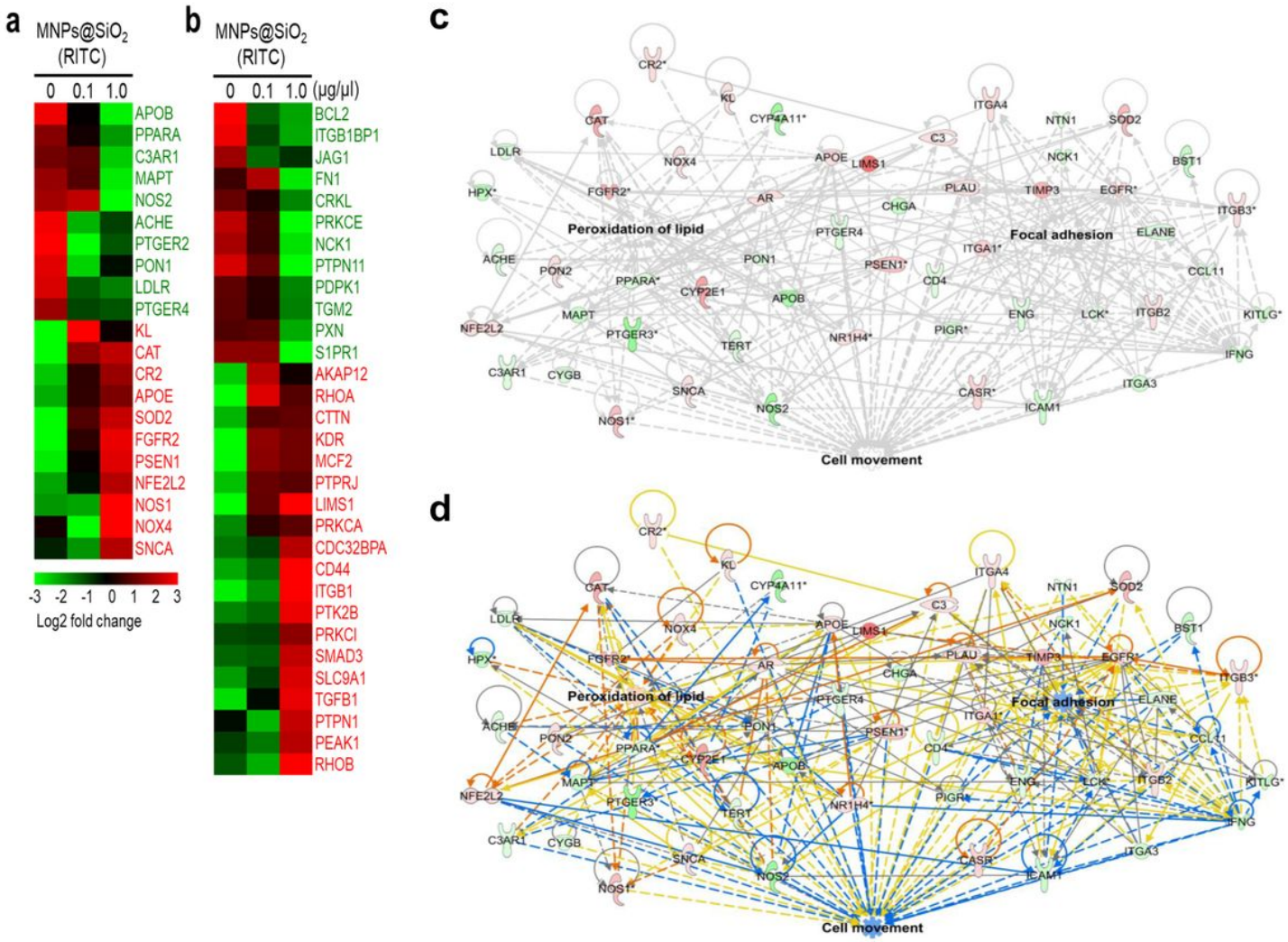

Figure 5

Analysis of transcriptome in HEK293 cells treated with MNPs@SiO2(RITC) for 12 h. Heat map of genes with altered expression (21 genes related to lipid peroxidation (a) and 31 genes related to focal adhesion (b)) were differentially expressed at 0.1 and 1.0 μg/μl of MNPs@SiO2(RITC)-treated cells, in accordance to microarray analysis. Red and green areas indicate up- and downregulated genes, respectively. Network of lipid peroxidation and focal adhesion related genes was constructed algorithmically by IPA. (c) Transcriptome network of 1.0 μg/μl of MNPs@SiO2(RITC)-treated cells were shown and (d) prediction analysis for the network. Red and green areas indicate up- and downregulated genes, respectively. Orange and blue colors indicate activation and suppression, respectively. The lines indicate indirect (dotted) or direct (solid) relationship. Differentially expressed genes obtained from microarray data (genes with > 3-fold change) are shown.

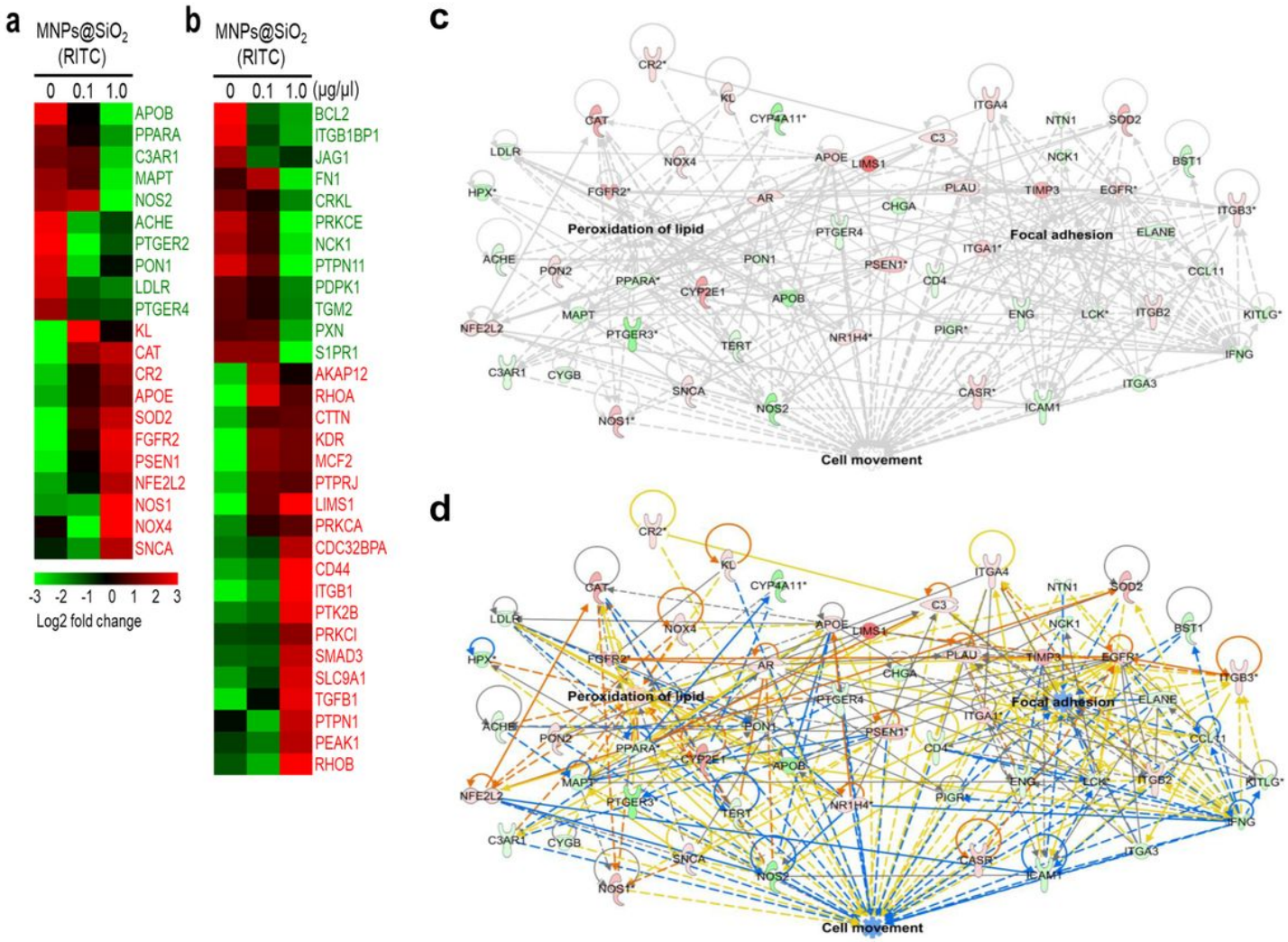

Figure 5

Analysis of transcriptome in HEK293 cells treated with MNPs@SiO2(RITC) for 12 h. Heat map of genes with altered expression (21 genes related to lipid peroxidation (a) and 31 genes related to focal adhesion (b)) were differentially expressed at 0.1 and 1.0 μg/μl of MNPs@SiO2(RITC)-treated cells, in accordance to microarray analysis. Red and green areas indicate up- and downregulated genes, respectively. Network of lipid peroxidation and focal adhesion related genes was constructed algorithmically by IPA. (c) Transcriptome network of 1.0 μg/μl of MNPs@SiO2(RITC)-treated cells were shown and (d) prediction analysis for the network. Red and green areas indicate up- and downregulated genes, respectively. Orange and blue colors indicate activation and suppression, respectively. The lines indicate indirect (dotted) or direct (solid) relationship. Differentially expressed genes obtained from microarray data (genes with > 3-fold change) are shown.

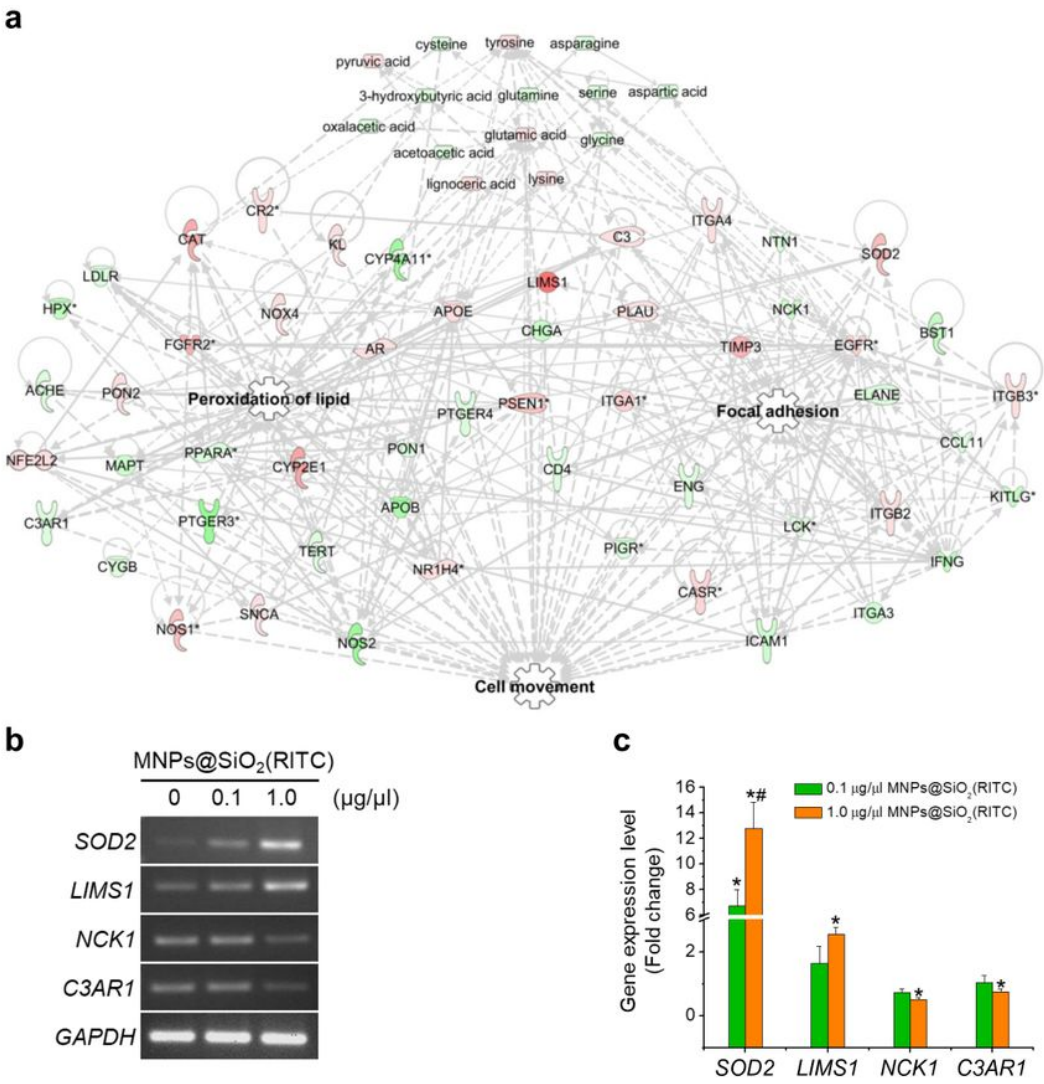

Figure 6

Metabotranscriptomic analysis of the microarray and metabolite profile of MNPs@SiO2(RITC)-treated cells. (a) Lipid peroxidation and focal adhesion-related genes and metabolite networks were algorithmically constructed using IPA. Red and green areas indicate up- and downregulated genes, respectively. The lines indicate indirect (dotted) or direct (solid) relationship. Differentially expressed genes obtained from microarray data (>3-fold change) and disturbances in the metabolic profile (>20% change) are shown. (b, c) Quantitative evaluation of the metabotranscriptomic network-related genes by semi-quantitative reverse transcription (RT)-PCR and quantitative real-time (q)PCR. Cells were treated with 0.1 and 1.0 μg/μl MNPs@SiO2(RITC) for 12 h. RT-PCR and qPCR were performed using gene-specific primer pairs for SOD2, LIMS1, NCK1, and C3AR1. GAPDH was used as the internal control. PCR products were normalized relative to the levels of internal control. Data represent the means ± SD of three independent experiments. *p < 0.05 vs non-treated control. Transcriptome and metabolome data are reproduced from our previous study, Copyright © 2019 Springer Nature [37].

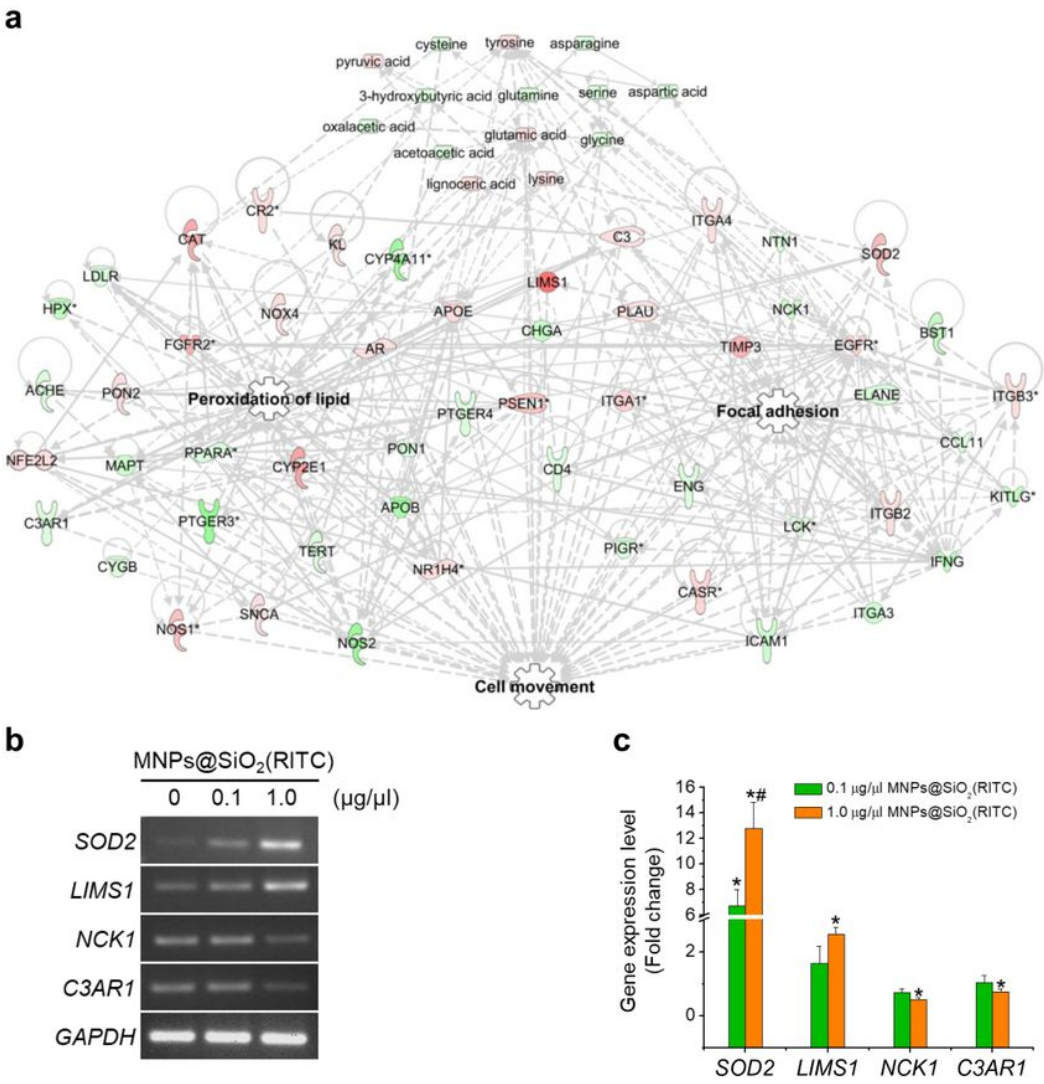

Figure 6

Metabotranscriptomic analysis of the microarray and metabolite profile of MNPs@SiO2(RITC)-treated cells. (a) Lipid peroxidation and focal adhesion-related genes and metabolite networks were algorithmically constructed using IPA. Red and green areas indicate up- and downregulated genes, respectively. The lines indicate indirect (dotted) or direct (solid) relationship. Differentially expressed genes obtained from microarray data (>3-fold change) and disturbances in the metabolic profile (>20% change) are shown. (b, c) Quantitative evaluation of the metabotranscriptomic network-related genes by semi-quantitative reverse transcription (RT)-PCR and quantitative real-time (q)PCR. Cells were treated with 0.1 and 1.0 μg/μl MNPs@SiO2(RITC) for 12 h. RT-PCR and qPCR were performed using gene-specific primer pairs for SOD2, LIMS1, NCK1, and C3AR1. GAPDH was used as the internal control. PCR products were normalized relative to the levels of internal control. Data represent the means ± SD of three independent experiments. *p < 0.05 vs non-treated control. Transcriptome and metabolome data are reproduced from our previous study, Copyright © 2019 Springer Nature [37].

Supplementary Files

This is a list of supplementary files associated with this preprint. Click to download.

- AdditionalFile1.docx
- AdditionalFile1.docx
- AdditionalFile2MovieS1.avi
- AdditionalFile2MovieS1.avi
- AdditionalFile2MovieS2.avi
- AdditionalFile2MovieS2.avi
- AdditionalFile2MovieS3.avi
- AdditionalFile2MovieS3.avi